Monte Carlo computer simulation of order-order kinetics in the $L1_2$-ordered Ni_3Al binary system

P. Oramus and R. Kozubski
Institute of Physics, Jagellonian University, Reymonta 4, 30-059 Krakow, Poland

V. Pierron-Bohnes and M. C. Cadeville
Institut de Physique et Chimie des Materiaux de Strasbourg, 23, rue du Loess, 67037 Strasbourg, France

W. Pfeiler
Institut fur Materialphysik, University of Vienna, Strudlhofgasse 4, A-1090 Vienna, Austria
(Received 27 May 2000; revised manuscript received 15 December 2000; published 9 April 2001)

The results of previous extensive experiments on γ'-Ni_3Al systems are interpreted and explained by means of Monte Carlo computer simulations based on the Glauber algorithm for vacancy mechanism of atomic migration in a superstructure. The complex character of the experimental ''order-order'' relaxation curves, as well as the theoretically predicted effect of vacancy ordering have been perfectly reproduced and analyzed in detail in terms of the dynamics of particular kinds of atomic jumps. The relaxations corresponding to an increase and decrease of the degree of long-range order showed up as processes only partially symmetric in time. The proposed model scenario for the creation and elimination of antisite atoms in the relaxing $L1_2$-type superstructure shows that the experimentally observed features of the ''order-order'' processes in Ni_3Al follow from an interplay between two dominating and coupled modes of long- and short-range ordering.

DOI: 10.1103/PhysRevB.63.174109 PACS number(s): 02.70.Uu, 61.72.Cc, 64.60.Cn, 81.30.Hd

I. INTRODUCTION

If a long-range ordered system annealed at temperature T_i is abruptly cooled down or heated up to temperature T_f, the degree η of its long-range order (LRO), i.e., the number of antisite atoms, evolves from the initial equilibrium value $\eta^{(eq)}(T_i)$ to the final one $\eta^{(eq)}(T_f)$. If both T_i and T_f temperatures are lower than the ''order-disorder'' transition point T_t, the process is called an ''order-order'' relaxation.

Because of an important effect of LRO on many physical and technological properties of metallic materials, ''order-order'' relaxations have been experimentally investigated for many years (for a review see, e.g., Ref. 1). Only recently, however, the process has been studied in high-temperature superalloys[1–5] representing so-called ''directly ordering systems,''[6] which show homogeneous superstructure with relatively low density of structural defects up to the melting point. ''Order-order'' relaxations in such systems are thus reasonably tractable as having the same mechanism as volume diffusion, i.e., elementary jumps of atoms to neighboring vacancies in bulk superstructure. Having similar mechanisms, the processes differ, however, in the character of correlations of elementary atomic jumps. While in the case of a steady-state diffusion in a superstructure atomic jumps are correlated in the way, that in average the degree of LRO is not disturbed, the ''order-order'' relaxation aims just at the change of η and requires different correlations. Studies of ''order-order'' relaxations and steady-state diffusion yield, therefore, complementary information on the dynamics of atomic migration in ordered crystals.[1,7]

Theoretical approaches to LRO relaxations based on fundamental kinetic equations have been reviewed in Ref. 1. Due to computational limitations, applicable conclusions following either from analytical or even numerical solutions of kinetic equations have so far been obtainable only for selected types of superstructures or specific thermodynamic conditions. However, implementation of general physical concepts with molecular dynamics (MD) or Monte Carlo (MC) computer simulation techniques allows a wide range of LRO kinetic problems to be studied.

Offering a possibility for investigating atomic migration in terms of crystal energetics treated by means of advanced solid-state theories, MD simulations are, however, technically limited to rather small samples and short periods of real time. Consequently, being very powerful when considering the dynamics of single atoms in a solid,[8] the method is less useful for studying net kinetic effects—such as, e.g., LRO relaxation.

Most of simulation studies of structural kinetics are thus carried out by means of the MC technique (for references see numerous works of Binder, e.g., Ref. 9). The method is based on numerical realisation of atomic jumps in a simulated system with probabilities defined in such a way that correct thermodynamics of the system is reproduced, i.e., the simulated system always relaxes to the state of thermodynamic equilibrium. The probabilities should depend on two factors: (i) driving force accounting for the effect of particular jumps on thermodynamic potential of the system and (ii) detailed energetics of a single jump including the saddle-point energy to be overcome by an atom when changing a position. While the first factor definitely determines the thermodynamical correctness of the model, the second one influences the details of the simulated kinetics.

Early models of Metropolis[10] and Glauber[11] accounted correctly for the effect of driving force, but neglected totally the saddle-point energy. In the case of Glauber, the probabil-

ity $\Pi_{i\to j}$ for an atomic jump from a site ''i'' to ''j'' is given by

$$\Pi_{i\to j}=\frac{\exp\left[\frac{-\Delta E}{kT}\right]}{1+\exp\left[\frac{-\Delta E}{kT}\right]} \tag{1.1}$$

where $\Delta E=E_j-E_i$, E_i and E_j denoting the system energies before and after the jump, respectively, k and T are Boltzmann constant and absolute temperature, respectively.

The probability $\Pi_{i\to j}$ defined by Eq. (1.1) is ''automatically'' normalized with respect to whether an atom executes the $i\to j$ jump or not. Since the pioneering papers on MC simulation of atomic migration processes[12,13] the Metropolis and Glauber algorithms have been commonly used in this sort of studies.[14–18] ΔE may be evaluated within the variety of existing models of crystalline systems including ''*ab initio*'' calculations.

An alternative algorithm accounting for and focusing on the effect of driving force refers to a general Onsager-type microscope diffusion equation proposed by Khachaturyan[19] and applied in simulation studies (see, e.g., Refs. 20–22):

$$\frac{dn(\vec{r},t)}{dt}=\sum_{\vec{r}'}\frac{L(\vec{r}-\vec{r}')}{kT}\times\frac{\delta F}{\delta n(\vec{r}',t)} \tag{1.2}$$

where $n(\vec{r},t)$ is an occupation parameter of the lattice site at $\vec{r}$, $L(\vec{r}-\vec{r}')$ is a kinetic coefficient, F is free energy and t, k, and T are time, Boltzmann constant, and temperature, respectively.

Saddle-point energy E^+ is usually introduced to the MC simulation algorithm by postulating

$$\Pi_{i\to j}=A\times\nu_0\times\exp\left[-\frac{E^+-E_i}{kT}\right], \tag{1.3}$$

where $\Pi_{i\to j}$ denotes again the probability for an atomic jump from a site ''i'' to ''j,'' E_i is the system energy before the jump, ν_0 is the attempt frequency of the jumping atom, and A is the normalization factor. Although such a definition of $\Pi_{i\to j}$ seems more adequate for the dynamics of atomic jumps, the advantage of the resulting algorithm over the ''classical'' one [Eq. (1.1)] has never been verified by systematic comparative simulation studies related to experimental results. On the other hand, the evident drawback of the approach consists of a general unavailability of actual values of saddle-point energies and consequently, E^+ is most often estimated by multiplying pair-interaction energies of nearest-neighboring atoms occupying lattice sites by arbitrary factors (see, e.g., Refs. 23,24) or by setting it as a phenomenological parameter depending only on the kind of the jumping atom (see, e.g., Refs. 14,25). Atomic migration may be effectively simulated by implementing particular formulas for the jump probabilities with a simulation algorithm, which defines the mechanism of the process (e.g., vacancy mechanism) and also its time scale.[26]

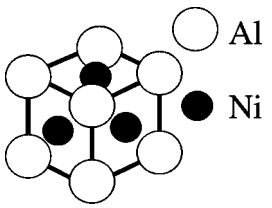

FIG. 1. Unit cell of $L1_2$-type superstructure of Ni_3Al.

Basic limitation of computer simulations of kinetics of processes controlled by atomic migration with vacancy mechanism is due to usual impossibility of a simulation of a system with realistic concentration c_v of thermal vacancies (because of a limited size of the simulated sample). This applies, e.g., to high-temperature intermetallics, where, at temperatures of measurable order-order relaxations, c_v is of the range of 10^{-9} (see, e.g., Ref. 27). This means that simulation of complete configurational kinetics is almost never feasible—i.e., there is no access to the vacancy formation energy, which substantially contributes to the real overall dynamics of the process.

The present Monte Carlo simulation study concerns order-order relaxations in a homogeneous A_3B binary system with a superstructure of $L1_2$ type and refers to the previous experimental works on Ni_3Al reviewed in Ref. 1. The interest is focused on the origin of the complex character of the $\eta(t)$ relaxation isotherms measured by means of residual resistometry, which fitted weighted sums of exactly two single exponentials with substantially different relaxation times. Preliminary results of the study have been presented in several international conferences.[28,29]

II. MONTE CARLO SIMULATION PROCEDURE

The sample was simulated by arranging two kinds of atom (Ni and Al) taken in a stoichiometric proportion $N_{\mathrm{Ni}}/N_{\mathrm{Al}}=3/1$ over a $L1_2$-type superlattice (Fig. 1) containing 256 000 sites. Subsequently, a fixed number of vacancies were introduced by emptying at random the corresponding number of lattice sites.

The equilibrium configuration of the system corresponding to a given temperature T was then generated by imposing periodic boundary conditions upon the system and letting it relax according to the following algorithm: random choice of one of the 12 lattice sites of the vacancy's first coordination shell, calculation (within a particular model) of the probability Π[Ni(Al)] [Eq. (1.1)] for an exchange between the vacancy and an Ni or Al atom occupying the chosen lattice site, generation of a random number $R\in\langle 0,1\rangle$ and execution ($R\leqslant\Pi$) or suppression ($R>\Pi$) of the jump. The procedure was sequentially run for all vacancies present in the sample. The simplest and most clear time scale was defined: a unit time (MC time) was assigned to each completion of the above cycle (MC step).

The regular order-order relaxations were simulated by pursuing the above procedure at temperature T_f starting from

a system previously equilibrated (be means of the same procedure) at another temperature T_i. All the results presented in the paper have been averaged over 20 independent realizations of the procedure. Those presented in earlier communications[28,29] corresponded to $T_i = 0$ K (disordering of a perfectly ordered A_3B system).

The Glauber formula [Eq. (1.1)] for the probabilities of Ni- and Al-atom jumps to nearest neighbor vacancies was used. The probability was automatically put equal to zero if the randomly chosen lattice site was occupied by another vacancy.

It is clear that the applied atomic-jump probability [Eq. (1.1)] does not account for possible differences between the attempt frequencies ν_0 [Eq. (1.3)] of the jumping Ni and Al atoms. Although there are no data for the attempt frequency of Al in γ'-Ni_3Al (data for Ni may be found in Refs. 30,31), this simplifying approximation is at least partially justified either by considering Ni and Al as impurities within a model of Neumann,[32] or by analyzing the existing experimental data for Ni and Al diffusion in pure Ni—as recently done by Pareige *et al.*[25] In both cases the ν_0 values result almost the same for Ni and Al.

III. MODEL OF THE Ni_3Al BINARY SYSTEM

A. Hamiltonian

Only the configurational part of the system energy was considered when evaluating the probabilities Π [Eq. (1.1)]. It was approximated by an Ising Hamiltonian with six energy parameters $V^{(\nu)}_{A\text{-}B}$ describing ''*A*-*B*'' atomic pair interactions (A,B=Ni,Al) between nearest-neighbor [NN, $\nu = 1$] and next-nearest-neighbor [NNN, $\nu = 2$] atoms. Atom-vacancy and vacancy-vacancy pair-interaction energies were equaled to zero. In order to approach the reality of Ni_3Al the parameters were evaluated according to the following criteria:

$$V^{(\nu)}_{\text{Ni-Ni}} = 2 \times V^{(\nu)}_{\text{Al-Al}} \tag{3.1}$$

the coefficient close to 2 between NN Ni-Ni and Al-Al interactions in Ni_3Al appears in theoretical consideration (e.g., pairwise bonding model[33]),

$$W^{(1)} = \frac{1}{4}[V^{(1)}_{\text{Ni-Ni}} + V^{(1)}_{\text{Al-Al}} - 2 \times V^{(1)}_{\text{Ni-Al}}] = 0.035 \text{ eV} \tag{3.2}$$

the value following from diffuse scattering experiments corresponding, however, to the approximation of four co ordination shells,[34]

$$W^{(2)} = \frac{1}{4}[V^{(2)}_{\text{Ni-Ni}} + V^{(2)}_{\text{Al-Al}} - 2 \times V^{(2)}_{\text{Ni-Al}}] = -0.0165 \text{ eV}. \tag{3.3}$$

The value adjusted in the applied two coordination shell approximation with a requirement that Eq. (3.2) is fulfilled and that the order-disorder transition point is close to the T_t extrapolated for Ni_3Al.[6]

The acceptable sets of the pair-interaction energy parameters were thus definitely parametrized by only two independent quantities, e.g., $V^{(1)}_{\text{Al-Al}}$ and $V^{(2)}_{\text{Al-Al}}$.

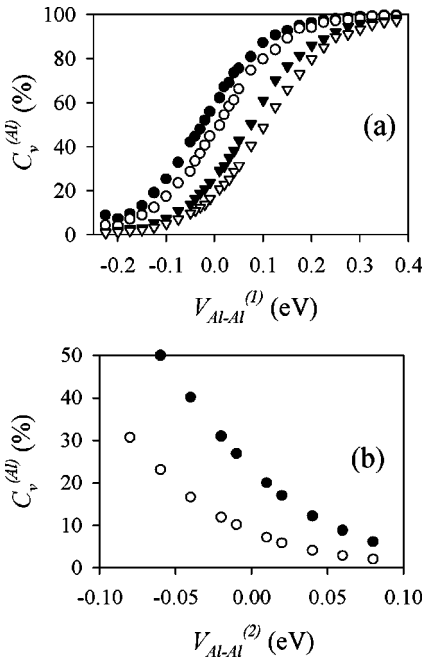

FIG. 2. Fraction of vacancies $C_v^{(\text{Al})}$ residing on Al sublattice against atomic pair-interaction energy parameters (a) $V^{(2)}_{\text{Al-Al}} = -0.04$ eV (●), $V^{(2)}_{\text{Al-Al}} = -0.02$ eV (○), $V^{(2)}_{\text{Al-Al}} = +0.02$ eV (▼), $V^{(2)}_{\text{Al-Al}} = +0.04$ eV (▽); (b) $V^{(1)}_{\text{Al-Al}} = -0.05$ eV (●), $V^{(1)}_{\text{Al-Al}} = -0.15$ eV (○).

It is commonly accepted that thermal vacancies in Ni_3Al occupy predominantly the Ni sublattice (see, e.g., Ref. 27 and related references therein). Preliminary simulation runs showed that vacancies (initially distributed at random) drifted towards particular sublattice sites. The rate of this drift was by an order of magnitude higher than the rate of any order-order relaxation. The final vacancy distribution in the sample depends on the applied atomic pair-interaction energy parameters fulfilling the criteria of Eqs. (3.1)–(3.3) [Figs. 2(a),2(b)]. Consequently, in order to keep up with the reality of Ni_3Al, i.e., to make less than 25% of all vacancies reside in equilibrium on the Al sublattice, all further simulations were run with $V^{(1)}_{\text{Al-Al}} = -0.15$ eV or $V^{(1)}_{\text{Al-Al}} = -0.05$ eV and with $V^{(2)}_{\text{Al-Al}}$ varied between -0.06 and $+0.08$ eV.

B. Vacancy concentration

An introduction of one single vacancy to the simulated sample means the vacancy concentration $c_v \sim 10^{-5}$; the value by at least 3 orders of magnitude higher than the real one in Ni_3Al at temperature $T = 0.5 \times T_m$ (i.e., within the range of measurable order-order relaxations[1]). Therefore, the actual number of vacancies in the system had no but purely technical meaning affecting the time scale (relaxation rate) of simulated order-order relaxations.

The effect has two aspects: (1) according to the definition of MC time the relaxation rate at given temperature should be proportional to c_v, (2) an increase of c_v should slow the relaxation down due to an increasing concentration of divacancies (or even larger vacancy clusters) and the resulting

TABLE I. Meaning of atomic-jump frequency parameters $P_{\mathrm{Ni(Al)}:i\to j}$.

Symbol	Meaning	Jump effect
$P_{\mathrm{Ni:Al}\to\mathrm{Ni}}$	Ni-atom jump from Al-sublattice site to a NN vacancy residing on Ni-sublattice site	ordering
$P_{\mathrm{Ni:Ni}\to\mathrm{Al}}$	Ni-atom jump from Ni-sublattice site to a NN vacancy residing on Al-sublattice site	disordering
$P_{\mathrm{Ni:Ni}\to\mathrm{Ni}}$	Ni-atom jump from Ni-sublattice site to a NN vacancy residing on Ni-sublattice site	no effect
$P_{\mathrm{Al:Ni}\to\mathrm{Al}}$	Al-atom jump from Ni-sublattice site to a NN vacancy residing on Al-sublattice site	ordering
$P_{\mathrm{Al:Al}\to\mathrm{Ni}}$	Al-atom jump from Al-sublattice site to a NN vacancy residing on Ni-sublattice site	disordering
$P_{\mathrm{Al:Ni}\to\mathrm{Ni}}$	Al-atom jump from Ni-sublattice site to a NN vacancy residing on Ni-sublattice site	coupling and uncoupling of NN antisite pairs

increase of the number of ''lost'' MC steps [$\Pi=0$ in Eq. (1.1)]. It has been shown that as long as c_v is reasonably small (i.e., does not exceed about 10^{-3}), the relaxation rates are proportional to c_v. Consequently, the value of c_v may be chosen arbitrarily (within a reasonable range) without loosing the physical meaning of the simulated order-order relaxations. All over the presented work the simulated sample contained 10 vacancies.

C. Monitored parameters

The current configuration of the system was analyzed within specifically extended point approximation involving the following three parameters.

(i) A Bragg-Williams-type LRO parameter η

$$\eta=1-\frac{N_{\mathrm{Ni}}^{(\mathrm{Al})}}{0.75\times N^{(\mathrm{Al})}}, \tag{3.4}$$

where $N^{(\mathrm{Al})}$ and $N_{\mathrm{Ni}}^{(\mathrm{Al})}$ denote the number of Al-type sublattice sites and the number of Ni antisites (Ni atoms on the Al sublattice), respectively.

(ii) A specific short-range-order-(SRO) type parameter antisite pair correlation (APC):

$$\mathrm{APC}=\frac{N_{\mathrm{NiAl}}^{(\mathrm{Al})(\mathrm{Ni})}}{N_{\mathrm{Ni}}^{(\mathrm{Al})}}, \tag{3.5}$$

where $N_{\mathrm{NiAl}}^{(\mathrm{Al})(\mathrm{Ni})}$ denotes the number of NN pairs of Ni and Al antisites.

(iii) Normalized average minimum distance $\langle r_{\mathrm{min}}\rangle_{\mathrm{nor}}$ between Ni and Al antisites

$$\langle r_{\mathrm{min}}\rangle_{\mathrm{nor}}=\frac{\langle r_{\mathrm{min}}\rangle}{r_{\mathrm{NN}}}, \tag{3.6}$$

where $\langle r_{\mathrm{min}}\rangle$ is a minimum distance between Ni and Al antisites averaged over all Al antisites and r_{NN} is the NN distance in the lattice. As the simulated order-order relaxations occurred in a homogeneously and nearly perfectly ordered system with no antiphase boundaries, it was sufficient to parametrize the state of LRO by means of one single LRO parameter instead of three, necessary for a full description of $L1_2$ type LRO in a binary system.

The order-order relaxations were investigated by monitoring the MC-time dependence of η, APC, and $\langle r_{\mathrm{min}}\rangle_{\mathrm{nor}}$ as well as by considering the jump-frequency parameters $P_{\mathrm{Ni(Al)}:i\to j}$:

$$P_{\mathrm{Ni(Al)}:i\to j}=\frac{N_{\mathrm{Ni(Al)}:i\to j}^{\mathrm{exec}}}{N_{\mathrm{att}}}, \tag{3.7}$$

where: $N_{\mathrm{Ni(Al)}:i\to j}^{\mathrm{exec}}$ denotes a number of Ni(Al)-atom jumps from an *i*-type sublattice site to a NN vacancy residing on *j*-type sublattice *executed* within a fixed number of MC steps, N_{att} denotes the total number of *jump attempts* (executed and not executed) during the same MC-time period.

Table I lists the parameters $P_{\mathrm{Ni(Al)}:i\to j}$ and indicates the role of corresponding atomic jumps in the order-order relaxation. As any atomic jump is ''reversed'' with a finite probability, i.e., after having jumped to a NN vacancy, the atom may subsequently jump back to its former position, it is reasonable to consider in addition the efficiency of particular ordering-disordering jumps

$$E_{\mathrm{Ni}}^{\mathrm{ord}}=\frac{P_{\mathrm{Ni:Al}\to\mathrm{Ni}}-P_{\mathrm{Ni:Ni}\to\mathrm{Al}}}{P_{\mathrm{Ni:Al}\to\mathrm{Ni}}};\quad E_{\mathrm{Ni}}^{\mathrm{dis}}=\frac{P_{\mathrm{Ni:Ni}\to\mathrm{Al}}-P_{\mathrm{Ni:Al}\to\mathrm{Ni}}}{P_{\mathrm{Ni:Ni}\to\mathrm{Al}}},$$

$$E_{\mathrm{Al}}^{\mathrm{ord}}=\frac{P_{\mathrm{Al:Ni}\to\mathrm{Al}}-P_{\mathrm{Al:Al}\to\mathrm{Ni}}}{P_{\mathrm{Al:Ni}\to\mathrm{Al}}};\quad E_{\mathrm{Al}}^{\mathrm{dis}}=\frac{P_{\mathrm{Al:Al}\to\mathrm{Ni}}-P_{\mathrm{Al:Ni}\to\mathrm{Al}}}{P_{\mathrm{Al:Al}\to\mathrm{Ni}}}. \tag{3.8}$$

IV. RESULTS

A. Stability of $L1_2$ superstructure of Ni_3Al

An example of the temperature dependence of the simulated equilibrium value of η obtained for one of the acceptable sets of $V_{A\text{-}B}^{(\nu)}$ is displayed in Fig. 3. Qualitatively similar behavior of $\eta^{(\mathrm{eq})}(T)$ curves was observed for each applied set of $V_{A\text{-}B}^{(\nu)}$: the $\eta^{(\mathrm{eq})}(T)$ curves dropped discontinuously down to $\eta^{(\mathrm{eq})}=0$ at $T_c\approx 1720$ K, as expected.

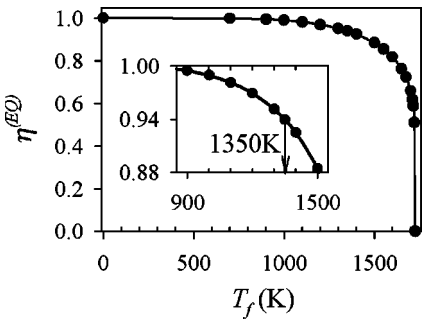

FIG. 3. Temperature dependence of the equilibrium value $\eta^{(\mathrm{eq})}$ of LRO parameter in Ni_3Al simulated at $V^{(1)}_{\mathrm{Al\text{-}Al}}=-0.15$ eV and $V^{(2)}_{\mathrm{Al\text{-}Al}}=-0.04$ eV. The inset shows the fragment corresponding to 900 K$<T<$1500 K and related to most of the simulations.

B. ''Order-order'' relaxations

1. General features of the relaxation curves

In general, a comparative study of disordering ($\Delta T=T_f-T_i>0$) and ordering ($\Delta T<0$) relaxations occurring at the same temperatures T_f was carried out. The temperatures T_i and T_f were chosen in the way that both the initial [$\eta(t=0)$] and final ($\eta^{(\mathrm{eq})}$) values of η were high and that the amplitudes $|\eta(t=0)-\eta^{(\mathrm{eq})}|$ of both ordering and disordering relaxations were low and equal. In practice, it appeared that no interpretable results were obtained if the relative amplitudes $|\eta(t=0)-\eta^{(\mathrm{eq})}|/\eta(t=0)$ were lower than 1%. A pair of qualitatively typical isotherms $\eta(t)$ obtained in this way is presented in Fig. 4(a). Laplace transformations of the isotherms revealed exactly two peaks in the relaxation-time distribution [Figs. 4(b), 4(c)], which directly refers to the experimental results previously reported for Ni_3Al.[1] Thus, the curves fitted approximately weighted sums of two single exponentials

$$\frac{\eta(t)-\eta^{(\mathrm{eq})}}{\eta(t=0)-\eta^{(\mathrm{eq})}}\approx C\times\exp\left[-\frac{t}{\tau_s}\right]+(1-C)\times\exp\left[-\frac{t}{\tau_l}\right];$$

$$\tau_l>\tau_s;\quad 0\leqslant C\leqslant 1, \tag{4.1}$$

where the two relaxation times τ_s and τ_l differed by up to a factor of 50.

While regular Arrhenius plots yielding effective positive activation energy E_A were obtained for the longer relaxation times τ_l (slow relaxation process), the shorter relaxation times τ_s showed no significant temperature dependence (Fig. 5). An analysis of the jump frequencies $P_{\mathrm{Ni(Al)}:i\to j}$ [Eq. (3.7)] showed that, as expected (fixed number of lattice sites and vacancies), exactly equal numbers of Ni and Al antisites were created or removed within any MC-time intervals during the simulated relaxations. Consequently, any possible ''unbalance'' between, e.g., $P_{\mathrm{Ni:Ni}\to\mathrm{Al}}$ and $P_{\mathrm{Al:Al}\to\mathrm{Ni}}$ caused by differences between the respective energy increments/decrements ΔE in Eq. (1.1), must have been compensated by an appropriate frequency of reversed jumps.

The general strategy for the whole further study consisted of a search for possible model parameters affecting or being correlated with the value of the weight factor C [Eq. (4.1)]. It was expected that by controlling C it would be possible to reveal the microscopic mechanism responsible for the observed structure of order-order relaxation process in Ni_3Al.

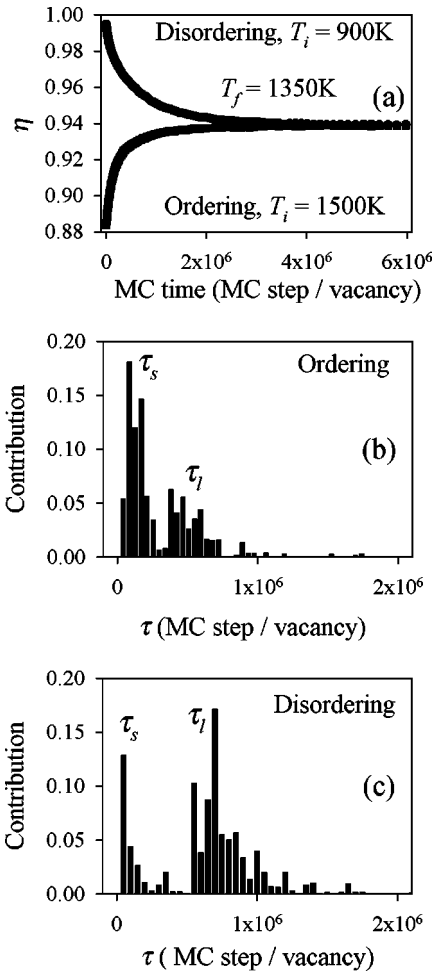

FIG. 4. (a) Ordering and disordering relaxation isotherms η(t) simulated at $V^{(1)}_{\mathrm{Al\text{-}Al}}=-0.15$ eV and $V^{(2)}_{\mathrm{Al\text{-}Al}}=-0.04$ eV, and at common $T_f=1350$ K. (b),(c) The related Laplace spectra of relaxation times.

2. Factors controlling the contribution of the fast process to the order-order relaxation

Analyzed were series of ordering ($\Delta T<0$) and disordering ($\Delta T>0$) relaxations occurring at fixed temperatures T_f (tests were repeated for different values of T_f). The weight factor C resulted always higher for ordering than for disordering and in both cases showed slight, though systematic decrease with increasing T_f.

The most important observation indicated, however, that both for ordering and disordering the value of C gradually decreased when, at fixed T_f and $V^{(1)}_{\mathrm{Al\text{-}Al}}$, the value of $V^{(2)}_{\mathrm{Al\text{-}Al}}$ was increased within the limits allowed by Eqs. (3.1)–(3.3) [Figs. 6(a),6(c)]. The changes of C were definitely more pronounced in the case of disordering relaxations, where it was possible to almost completely eliminate the fast process.

An increase of $V^{(2)}_{\mathrm{Al\text{-}Al}}$ (at fixed T_f and $V^{(1)}_{\mathrm{Al\text{-}Al}}$) influenced in completely different ways the two relaxation times τ_s and τ_l [Figs. 6(b),6(d)]: While the long one τ_l systematically in-

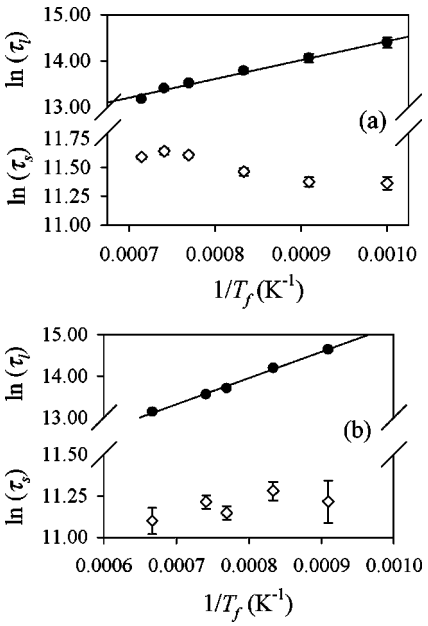

FIG. 5. Arrhenius plots of the rexation times τ_s ($\diamond$) and τ_l ($\bullet$) in (a) ordering and (b) disordering simulated at $V^{(1)}_{\text{Al-Al}}=-0.15$ eV and $V^{(2)}_{\text{Al-Al}}=-0.04$ eV.

creased both for ordering and disordering, τ_s slightly increased only for ordering and remained constant for disordering.

Isothermal relaxations of the LRO parameter η were accompanied by specific evolution of the SRO parameter APC [Eq. (3.5)] and $\langle r_{\min}\rangle_{\text{nor}}$ [Eq. (3.6)]. Figs. 7(a)–7(d) show examples of the MC-time dependence of APC and $\langle r_{\min}\rangle_{\text{nor}}$ corresponding to the $\eta(t)$ relaxations simulated at similar temperatures, but with different values of $V^{(2)}_{\text{Al-Al}}$ yielding different values of the weight factors *C*. In order to compare the rates of evolution of APC, $\langle r_{\min}\rangle_{\text{nor}}$ and η, the curves are shown together with the fast component of $\eta(t)$ (as τ_s depends very weakly on $V^{(2)}_{\text{Al-Al}}$ a comparison to one representative curve is sufficient).

In all cases, APC and $\langle r_{\min}\rangle_{\text{nor}}$ relaxed towards equilibrium levels APC$^{(\text{eq})}$ and $\langle r^{(\text{eq})}_{\min}\rangle_{\text{nor}}$, which for fixed T_f were common for all applied values of $V^{(2)}_{\text{Al-Al}}$ (i.e., for all observed values of *C*). Figure 8 shows APC$^{(\text{eq})}$ and $\langle r^{(\text{eq})}_{\min}\rangle_{\text{nor}}$ as functions of T_f.

At $\Delta T<0$ (ordering) APC and $\langle r_{\min}\rangle_{\text{nor}}$ relaxed towards the equilibrium levels by decreasing and increasing, respectively [Figs. 7(a),7(b)]. Although APC and $\langle r_{\min}\rangle_{\text{nor}}$ always reached their equilibrium levels far before the final saturation of $\eta(t)$, their relaxation rates were the lower, the lower was the value of the weight factor *C* connected with the corresponding $\eta(t)$ curve. In the case of the highest *C*, the relaxations of APC and $\langle r_{\min}\rangle_{\text{nor}}$ showed slight overshootings and proceeded with almost the same rates as did the fast component of $\eta(t)$.

In the case of $\Delta T>0$ (disordering) the overshootings were much stronger: an initial increase of APC (decrease of $\langle r_{\min}\rangle_{\text{nor}}$) led to a maximum value APC$_{\max}$ (minimum $\langle r_{\min}\rangle_{\text{nor}}$) and was followed by a decrease of APC (slight increase of $\langle r_{\min}\rangle_{\text{nor}}$) [Figs. 7(c) and 7(d)]. As follows from

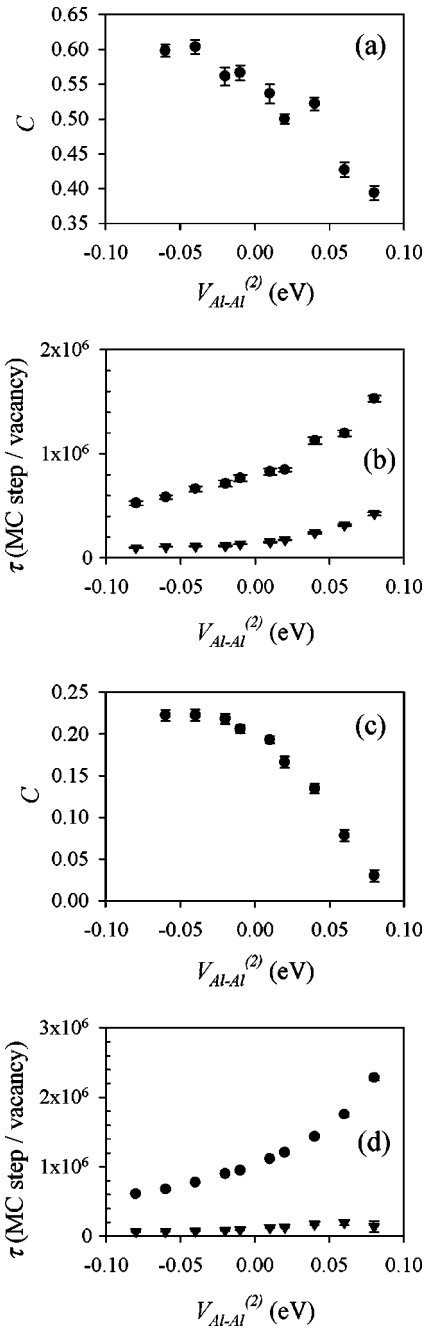

FIG. 6. Effect of $V^{(2)}_{\text{Al-Al}}$ on the value of the weight-factor *C* and the relaxation times τ_s ($\blacktriangledown$) and τ_l ($\bullet$) at $V^{(1)}_{\text{Al-Al}}=-0.15$ eV: (a), (b) ordering at $T_i=1500$ K, $T_f=1350$ K; (c), (d) disordering at $T_i=900$ K, $T_f=1350$ K.

the graphs, the higher was the value of the weight factor *C* of the corresponding $\eta(t)$ curve, the higher was APC$_{\max}$ and the lower was the minimum value of $\langle r_{\min}\rangle_{\text{nor}}$. The rate, at which the APC(t) and $\langle r_{\min}\rangle_{\text{nor}}(t)$ curves saturated, though decreasing with decreasing *C*, was always comparable with the rate, at which there saturated the fast component of $\eta(t)$.

3. Atomic-jump-scale analysis of order-order relaxations with various values of the weight factor C

The analysis consisted on a detailed inspection of the relationships between the atomic-jump-frequencies $P_{\text{Ni(Al)}:i\rightarrow j}$

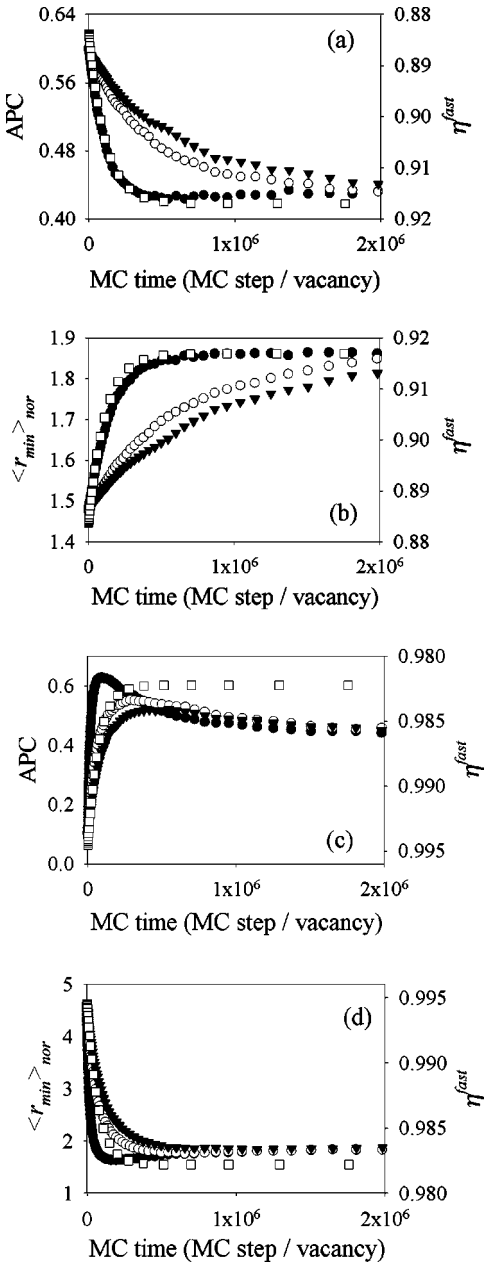

FIG. 7. APC and $\langle r_{\min}\rangle_{\mathrm{nor}}$ against MC-time during isothermal order-order relaxations. (a), (b) Ordering at $T_i=1500$ K, $T_f=1350$ K with $C=0.6$ (●), $C=0.43$ (○), $C=0.39$ (▼); (c), (d) disordering at $T_i=900$ K, $T_f=1350$ K with $C=0.22$ (●), $C=0.08$ (○), $C=0.03$ (▼). Fast component η^{fast} of η(t) at $C=0.6$ (a), (b) and $C=0.22$ (c), (d) is traced with □.

[Eq. (3.7)], efficiencies $E^{\mathrm{ord(dis)}}_{\mathrm{Ni(Al)}}$ [(3.8)] and the energetics of the system represented by the pair-interaction energies $V^{(2)}_{\mathrm{Al\text{-}Al}}$ correlated to the weightfactor C (see the previous paragraph). Considered were (a) $V^{(2)}_{\mathrm{Al\text{-}Al}}$ dependence of $P_{\mathrm{Ni(Al)}:i\rightarrow j}$ and $E^{\mathrm{ord(dis)}}_{\mathrm{Ni(Al)}}$ calculated within the first 5000 MC steps per vacancy, i.e., within the MC-time period shorter by an order of magnitude than the shortest relaxation time observed in any performed simulation, but covering the highest activity of the fast process and (b) evolution of $P_{\mathrm{Ni(Al)}:i\rightarrow j}$ and $E^{\mathrm{ord(dis)}}_{\mathrm{Ni(Al)}}$ during entire relaxation processes exhibiting extreme observed values of C.

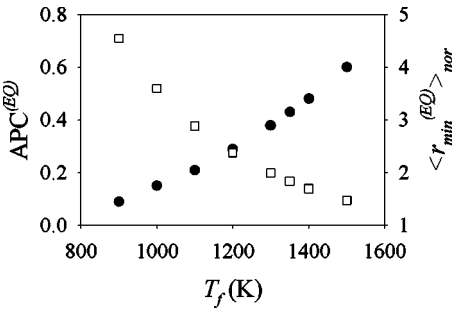

FIG. 8. Temperature dependence of $\mathrm{APC}^{(\mathrm{eq})}$ (●) and $\langle r^{(\mathrm{eq})}_{\mathrm{min}}\rangle_{\mathrm{nor}}$ (□) in Ni_3Al at $V^{(1)}_{\mathrm{Al\text{-}Al}}=-0.15$ eV and $V^{(2)}_{\mathrm{Al\text{-}Al}}=-0.04$ eV.

The general and obviously expected feature of all analyzed relaxations was a definite domination of Ni-atom jumps within Ni sublattice: $P_{\mathrm{Ni:Ni}\rightarrow\mathrm{Ni}}$ was always about 30 times higher than any other frequency and almost independent on $V^{(2)}_{\mathrm{Al\text{-}Al}}$ and T. Hence, it is not shown in the following diagrams.

(a) *Initial stages of relaxations.* The results are displayed in Fig. 9: In parallel with the frequencies $P_{\mathrm{Ni(Al)}:i\rightarrow j}$ [Figs. 9(a),9(d)] and efficiencies $E^{\mathrm{ord(dis)}}_{\mathrm{Ni(Al)}}$ [Figs. 9(b),9(e)] displayed together with $C(V^{(2)}_{\mathrm{Al\text{-}Al}})$, the $V^{(2)}_{\mathrm{Al\text{-}Al}}$ dependence of the system-energy changes ΔE corresponding to particular jumps [see Eq.(1.1)] and averaged over the same MC-time period as P and $E^{\mathrm{ord/dis}}$ is shown [Figs. 9(c),9(f)]. Both for ordering and disordering the weakest dependence on $V^{(2)}_{\mathrm{Al\text{-}Al}}$ was observed for $P_{\mathrm{Al:Ni}\rightarrow\mathrm{Ni}}$ (Al-antisite transportation via Ni sublattice). Considerably higher value of $P_{\mathrm{Al:Ni}\rightarrow\mathrm{Ni}}$ in the case of ordering obviously follows from the higher initial number of Al antisites present in the system.

Both for ordering ($\Delta T<0$) and disordering ($\Delta T>0$) an increase of $V^{(2)}_{\mathrm{Al\text{-}Al}}$ was accompanied by the following effects: decrease of the frequencies of ordering and disordering atomic jumps and, slight decrease of the efficiency $E^{\mathrm{ord/dis}}_{\mathrm{Ni}}$ of the ordering-disordering Ni-atom jumps and substantial increase of the efficiency $E^{\mathrm{ord/dis}}_{\mathrm{Al}}$ of the ordering-disordering Al-atom jumps.

It is interesting to consider the correlation of the variation of the jump frequencies [Figs. 9(a),9(d)] with the corresponding variation of the respective energy changes ΔE [Figs. 9(c),9(f)]. Although according to Eq. (1.1), the frequencies should decrease with increasing ΔE, this kind of behavior was observed, both for ordering and disordering, only for $P_{\mathrm{Ni:Al}\rightarrow\mathrm{Ni}}$ and $P_{\mathrm{Al:Al}\rightarrow\mathrm{Ni}}$, i.e., for the frequencies of jumps to Ni vacancies. As explained in Sec. V B, the anomaly resulted from a specific statistical correlation between the ordering-disordering jumps of Ni and Al atoms. It should finally be noted that the Ni-atom-jump frequencies (except for $P_{\mathrm{Ni:Ni}\rightarrow\mathrm{Ni}}$ not shown here) were considerably higher in the case of ordering than disordering.

(b) *Entire order-order relaxations with different values of C.* Figures 10 and 11 show the evolution of the atomic-jump frequencies and efficiencies during ordering and disordering relaxations simulated at $T_f=1350$ K for two extreme values of C, respectively. The jump frequencies are displayed

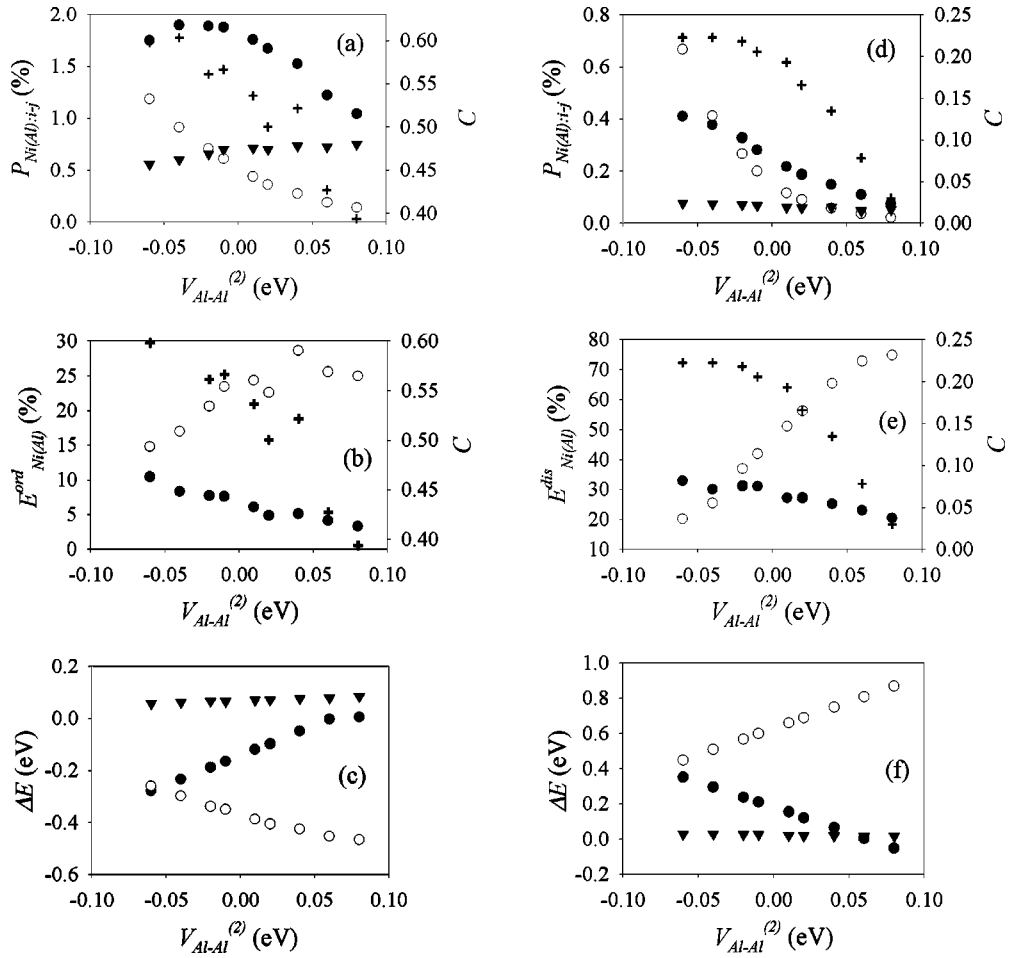

FIG. 9. Values of atomic-jump frequencies $P_{\mathrm{Ni(Al)}:i\to j}$, efficiencies $E^{\mathrm{ord/dis}}_{\mathrm{Ni(Al)}}$ and related average system-energy changes ΔE averaged over the first 5000 MC steps/vacancy against $V^{(2)}_{\mathrm{Al\text{-}Al}}$: (a), (b), (c) ordering at $T_i=1500$ K, $T_f=1350$ K, $P_{\mathrm{Ni:Al}\to\mathrm{Ni}}$ (●), $P_{\mathrm{Al:Ni}\to Al}$ (○), $P_{\mathrm{Al:Ni}\to\mathrm{Ni}}$ (▼); (d), (e), (f) disordering at $T_i=900$ K, $T_f=1350$ K, $P_{\mathrm{Ni:Ni}\to\mathrm{Al}}$ (●), $P_{\mathrm{Al:Al}\to\mathrm{Ni}}$ (○), $P_{\mathrm{Al:Ni}\to\mathrm{Ni}}$ (▼). $V^{(2)}_{\mathrm{Al\text{-}Al}}$ dependence of C [earlier shown in Figs. 6(a) and 6(c)] is traced in diagrams (a), (b), (d), and (e) with + symbols.

against η, because in this way the stages of relaxations are clearly visible.

Ordering with the highest C [Figs. 10(a) and 10(b)] proceeded with gradually decreasing jump frequencies of both Ni and Al atoms. The following relations were maintained all through the process: $P_{\mathrm{Ni:Al}\to\mathrm{Ni}}>P_{\mathrm{Al:Ni}\to\mathrm{Al}}>P_{\mathrm{Al:Ni}\to\mathrm{Ni}}$ and $E^{\mathrm{ord}}_{\mathrm{Al}}>E^{\mathrm{ord}}_{\mathrm{Ni}}$. While the process progressed, the differences between the jump frequencies and efficiencies definitely decreased.

Ordering with the lowest observed (though still high) C [Figs. 10(c) and 10(d)] differs from the latter case in considerably lower frequency $P_{\mathrm{Al:Ni}\to\mathrm{Al}}$ of the Al atom ordering jumps: $P_{\mathrm{Ni:Al}\to\mathrm{Ni}}>P_{\mathrm{Al:Ni}\to\mathrm{Ni}}>>P_{\mathrm{Al:Ni}\to\mathrm{Al}}$. It is, however, remarkable that the efficiencies $E^{\mathrm{ord}}_{\mathrm{Ni}}$ and $E^{\mathrm{ord}}_{\mathrm{Al}}$ of Ni- and Al-atom ordering jumps were substantially reduced and enhanced, respectively.

The analogous diagram corresponding to disordering with the highest observed C is more complex [Figs. 11(a) and 11(b)]. The relaxation started again with highly efficient disordering jumps with $P_{\mathrm{Al:Al}\to\mathrm{Ni}}>P_{\mathrm{Ni:Ni}\to\mathrm{Al}}$. While the process progressed, both disordering-jump frequencies $P_{\mathrm{Al:Al}\to\mathrm{Ni}}$ and $P_{\mathrm{Ni:Ni}\to\mathrm{Al}}$ increased, however, $P_{\mathrm{Ni:Ni}\to\mathrm{Al}}$ increased faster and quite soon became higher than $P_{\mathrm{Al:Al}\to\mathrm{Ni}}$. Both $P_{\mathrm{Al:Al}\to\mathrm{Ni}}$ and $P_{\mathrm{Ni:Ni}\to\mathrm{Al}}$ were all the time higher than $P_{\mathrm{Al:Ni}\to\mathrm{Ni}}$, which, however, also increased—apparently due to an increase of the number of Al antisites. The disordering-jump efficiencies $E^{\mathrm{dis}}_{\mathrm{Ni}}$ and $E^{\mathrm{dis}}_{\mathrm{Al}}$ gradually decreased, being, however, almost equal all through the relaxation.

In the case of the disordering relaxation with the lowest value of C (lower than 5%) [Figs. 11(c) and 11(d)], the frequencies of Ni- and Al-atom disordering jumps again increased and their efficiencies decreased with decreasing η, but the following relations were maintained all through the process $P_{\mathrm{Ni:Ni}\to\mathrm{Al}}>P_{\mathrm{Al:Ni}\to\mathrm{Ni}}>>P_{\mathrm{Al:Al}\to\mathrm{Ni}}$ and $E^{\mathrm{dis}}_{\mathrm{Al}}>E^{\mathrm{dis}}_{\mathrm{Ni}}$. Similarly as in the case of ordering, a decrease of C was followed by a considerable reduction of $P_{\mathrm{Al:Al}\to\mathrm{Ni}}$ and a substantial increase of $E^{\mathrm{dis}}_{\mathrm{Al}}$.

V. MODEL OF THE ORDER-ORDER RELAXATION PROCESS IN $L1_2$-ORDERED Ni_3Al SYSTEM

A. General remarks

The presented Monte Carlo simulation study of the order-order relaxations in the $L1_2$-ordered $A_3B(Ni_3Al)$ binary sys-

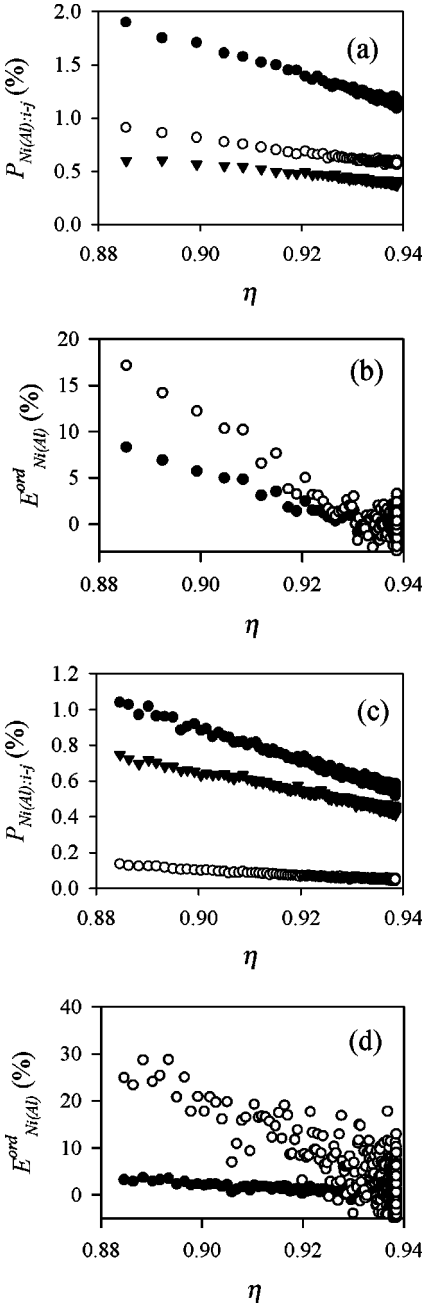

FIG. 10. Atomic-jump frequencies $P_{\mathrm{Ni(Al)}:i\rightarrow j}$ and efficiencies $E^{\mathrm{ord}}_{\mathrm{Ni(Al)}}$ against η during ordering at $T_i=1500$ K, $T_f=1350$ K with $C=0.6$ (a), (b) and $C=0.43$ (c), (d): $P_{\mathrm{Ni:Al}\rightarrow\mathrm{Ni}}$ (●), $P_{\mathrm{Al:Ni}\rightarrow Al}$ (○), $P_{\mathrm{Al:Ni}\rightarrow\mathrm{Ni}}$ (▼).

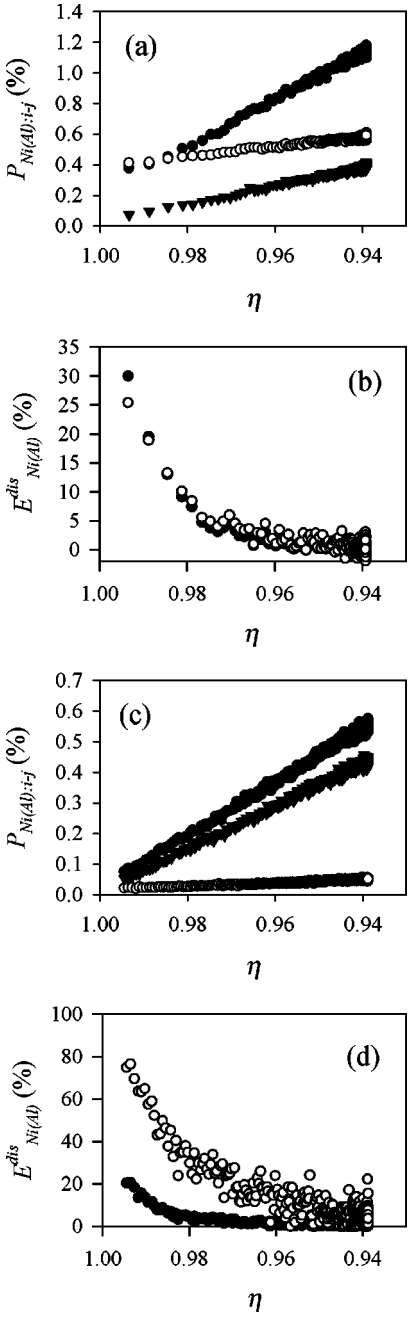

FIG. 11. Atomic-jump frequencies $P_{\mathrm{Ni(Al)}:i\rightarrow j}$ and efficiencies $E^{\mathrm{dis}}_{\mathrm{Ni(Al)}}$ against η during disordering at at $T_i=900$ K, $T_f=1350$ K with $C=0.22$ (a), (b) and $C=0.04$ (c), (d): $P_{\mathrm{Ni:Ni}\rightarrow\mathrm{Al}}$ (●), $P_{\mathrm{Al:Al}\rightarrow\mathrm{Ni}}$ (○), $P_{\mathrm{Al:Ni}\rightarrow\mathrm{Ni}}$ (▼).

tem offers a new insight into the microscopic mechanism of the process, which has up to now been only a subject of speculations in view of the experimental results.[1,4] An order-order relaxation is a complex cooperative process rearranging atomic configuration in the superstructure and thus, its full description involves the time evolution of all multisite correlation functions (see, e.g., Ref. 1 and references therein). In general, particular multisite correlation functions are coupled one with another and do not relax independently.

An interplay between the LRO and SRO relaxations were the subject of many theoretical studies carried out most often by means of the master equation method [(MEM), see, e.g., Refs. 35,36] or path probability method [(PPM), see, e.g., Ref. 37]. It was indicated that, in general, SRO relaxes substantially faster than does LRO. For a decade, the effect has been observable in direct experiments[38] concerning, however, in most cases order-disorder transformations.

The analysis presented in the present work involved the Bragg-Williams LRO parameter η and only one specific SRO parameter: the antisite NN pair-correlation APC. Thus, only a partial image of the phenomenon is given. The results shown in Fig. 7 indicate that the SRO (APC) relaxation

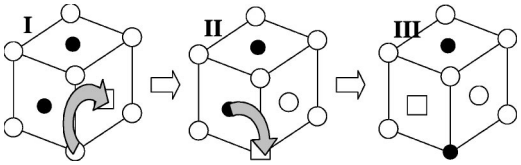

FIG. 12. Scheme of the formation of NN antisite pairs, the process of fast ordering and disordering in $L1_2$-ordered A_3B binary system: ●: *A* atoms ○: B-atoms, □: vacancy.

caused a fast change of LRO (η) and in this way generated the observed complexity of the overall isothermal time evolution of LRO (two simultaneous processes with different rates). The subsequent paragraphs are devoted to a description of the phenomenon in terms of the statistics of elementary atomic jumps in $L1_2$ sublattice.

B. Mechanism of the ''order-order'' relaxation process in $L1_2$-ordered Ni_3Al system

Taking into account the geometry of the $L1_2$ superstructure and, in addition, the fact that vacancies reside predominantly on the Ni sublattice, it is easy to conclude that the process of creation or elimination of NN antisite pairs is absolutely the most effective mode of ordering or disordering (elimination or creation of antisite atoms) in Ni_3Al. Each cycle of this process causes a substantial change of η by simultaneous production or elimination of two antisites and, what is more, starts and completes with a mobile Ni vacancy able to initiate another cycle (Fig. 12).

The role of NN antisite pairs in the order-order kinetics in an Ni_3Al $L1_2$-ordered system was additionally displayed by simulating ordering relaxations with artificially generated nonequilibrium initial APC. The $\eta(t)$ curves resulting from simulations with $T_i=1500$ K and $T_f=1350$ K are shown in Fig. 13. In the case of simulation started at equilibrium APC (open circles) the regular relaxation was observed. In the case of the initial value of APC equal to 1 (solid squares) the process of ordering was substantially enhanced and even overshot the equilibrium value of η. The case with APC initially equal to 0 (diamonds) turned out to be very interesting. Ordering was first suppressed, and even preceded by slight disordering connected with an increase of APC. Only

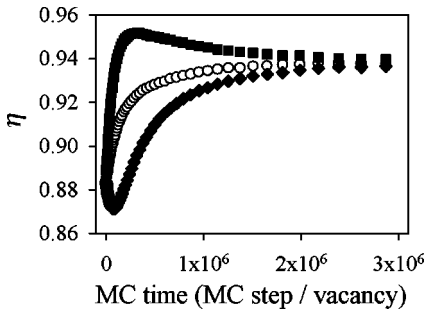

FIG. 13. $\eta(t)$ isotherms for ordering at $T_i=1500$ K, $T_f=1350$ K and at $V^{(1)}_{\text{Al-Al}}=-0.15$ eV and $V^{(2)}_{\text{Al-Al}}=-0.04$ eV with artificially generated extreme initial levels of APC: $\text{APC}_i=1$ (■), $\text{APC}_i=\text{APC}^{(\text{eq})}$ (1350 K) (○), $\text{APC}_i=0$ (◆).

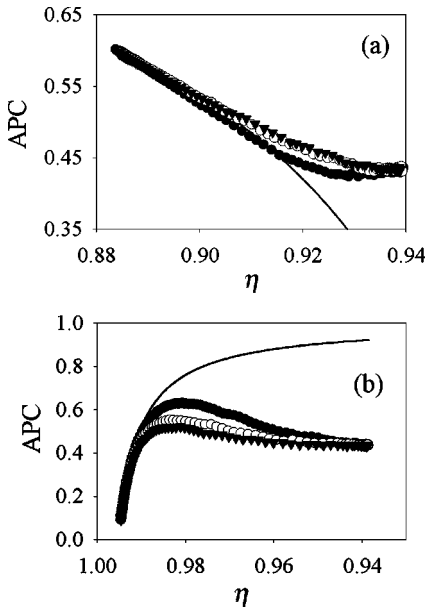

FIG. 14. APC against η during isothermal order-order relaxations. (a) Ordering at $T_i=1500$ K, $T_f=1350$ K with $C=0.6$ (●), $C=0.43$ (○), $C=0.39$ (▼); (b) disordering at $T_i=900$ K, $T_f=1350$ K with $C=0.22$ (●), $C=0.08$ (○), $C=0.03$ (▼). APC(η) curves following from Eq. (5.1) are traced as full lines.

after having produced a certain number of NN antisite pairs, was the system able to order—i.e., to reduce the number of antisite atoms.

Elimination and creation of NN antisite pairs may proceed not only by ordering or disordering of the system, but also by uncoupling and coupling the pairs due to Al-antisite migration within Ni sublattice. It is easy to show that if NN antisite pairs in Ni_3Al are created or eliminated *exclusively* due to creation or elimination of Ni and Al antisites, the parameters η and APC defined by Eqs. (3.4) and (3.5) fulfill the following relationship:

$$(1-\eta)\times(\text{APC}-1)=\text{const} \tag{5.1}$$

with the value of const determined by initial values of η and APC.

Figs. 14(a) and 14(b) show APC against η corresponding to ordering and disordering $\eta(t)$ relaxations with different values of *C*. The curves given by Eq. (5.1) almost perfectly coincide with the simulated ones in early stages of relaxations. Moreover, it is visible that (i) both for ordering and disordering the departure of APC(η) from the relationship of Eq. (5.1) occurs the earlier, the lower is the value of *C*, (ii) in the case of ordering the departure occurs substantially later than in the case of disordering. The results indicate that the effect of Al-antisite migration is practically invisible during the early stages of the order-order relaxations dominated by the fast process. However, it definitely shows up within the rest of the kinetics, becoming important the later, the higher is the value of the weight factor *C*.

As mentioned earlier, the relaxations of η and APC are coupled, but both parameters tend to respective equilibrium values corresponding to T_f temperature. While the relaxation

of η results composed of two simultaneous exponential processes (Fig. 4), the evolution of APC is more complex and shows certain overshooting before the saturation is attained (Fig. 7).

Figures 9–11 yield an atomistic explanation of observed effects. In general, they reflect the asymmetry of the $L1_2$ superlattice: while both Ni and Al atoms may jump between different sublattices modifying locally the state of atomic order, easy migration of atoms not affecting the atomic order occurs exclusively within the Ni sublattice and, therefore, applies only to regular Ni atoms and Al antisites. Ordering and disordering cases need separate discussions.

1. Ordering

The fast process which starts after decreasing the system temperature ($\Delta T<0$) consists of a quick elimination of NN antisite pairs *existing in the system* by Ni vacancies. In parallel, however, the NN antisite pairs are permanently coupled and uncoupled by the Al antisites migrating in Ni sublattice [Figs. 10(a),10(b)], which either join, or leave the Ni antisites. Such events cause certain energy change ΔE of the system (negative for joining and positive for leaving an Ni antisite). Its value, being in average independent on $V^{(2)}_{\text{Al-Al}}$, cannot be estimated by averaging the ΔE for Al-antisite migration [as done in Figs. 9(c) and 9(f)] as the cases of coupling or uncoupling are only a small fraction of all Al-antisite migration jumps. A hand calculus of the above energy change was made for $V^{(1)}_{\text{Al-Al}}=-0.15$ eV and $V^{(2)}_{\text{Al-Al}}$ varied between -0.06 and $+0.08$ eV assuming a perfectly ordered superlattice of Ni_3Al ($\eta=1$). The ΔE resulted strictly independent on $V^{(2)}_{\text{Al-Al}}$ and equal to ± 0.145 eV for uncoupling and coupling, respectively.

The slow ordering consists of the elimination of NN antisite pairs *currently created* by the above coupling process. Because of low probability of Al reversals (Al-disordering jumps) and higher probability of Ni reversals [see the related levels of ΔE in Fig. 9(c) and note that during a particular relaxation process ΔE for ordering jumps is *in average* equal to $(-1)\times\Delta E$ for their reversals, i.e., disordering jumps] the frequency of Ni-atom jumps is always higher than the frequency of Al-atom ones. The necessary equilibrium between the numbers of eliminated Ni and Al antisites is, however, maintained, because Ni atoms for most of time oscillate between two NN regular and antisite positions (low value of $E^{\text{ord}}_{\text{Ni}}$).

Each cycle of the elimination of a NN antisite pair is initiated by a jump of an Ni antisite, which produces an Al vacancy, to which there may jump the neighboring Al antisite. Alternatively, however, the jump to the Al vacancy may be executed by one of the more numerous NN Ni atoms [probabilities of both events are quite high, see the corresponding ΔE in Fig. 9(c)], which then oscillates between its regular and antisite positions engaging the available vacancies and increasing the frequency of inefficient ordering or disordering Ni-atom jumps. The probability of the latter event somewhat increases with a decrease of the difference between ΔE for Ni-atom ordering and their reversals [compare Figs. 9(b) and 9(c)]. This, however, means an increase of ΔE for Ni-atom ordering jumps [Fig. 9(c)] and causes an effective decrease of $P_{\text{Ni:Al}\rightarrow\text{Ni}}$ [Fig. 9(a)]. As expected, due to the vacancy engaging by oscillating Ni atoms, the effect is accompanied by a decrease of $P_{\text{Al:Ni}\rightarrow\text{Al}}$, which falls below the almost constant level of $P_{\text{Al:Ni}\rightarrow\text{Ni}}$. On the other hand, $E^{\text{ord}}_{\text{Al}}$ increases [Fig. 9(b)] due to an increase of ΔE for Al reversals. Consequently, the rate of the elimination of NN antisite pairs in both the fast and slow processes slightly decreases [see an increase of τ_s and τ_l in Fig. 6(b)]. However, because of no substantial change of $P_{\text{Al:Ni}\rightarrow\text{Ni}}$ (including the coupling jumps, whose ΔE does not depend on $V^{(2)}_{\text{Al-Al}}$), this leads effectively to a relative increase of the number of NN antisite pairs eliminated by the slow process (in relation to the fast one) and a decrease of C, in consistency with the $C(V^{(2)}_{\text{Al-Al}})$ dependence traced in Figs. 6(a), 9(a), and 9(b).

The most efficient elimination of *existing* NN antisite pairs (highest value of C) occurs, therefore, in the case of the highest efficiency $E^{\text{ord}}_{\text{Ni}}$ of Ni-atom ordering jumps. It leads to a slight APC overshooting and, therefore, the final stage of η relaxation proceeds as a purely slow process controlled by Al-antisite migration [compare Figs. 7(a), 7(b), and 10].

Finally, Figs. 15(a),15(b) show the T_f dependence of the $P_{\text{Ni(Al)}:i\rightarrow j}$ and $E^{\text{ord}}_{\text{Ni(Al)}}$ parameters averaged over 5000 MC steps/vacancy at the beginning of ordering proceeding with the highest value of C and after the MC-time period three times longer than the short relaxation time (corresponding to current T_f).

Within the initial 5000 MC steps/vacancy, the frequencies of all the ordering jumps inrease with inreasing T_f, but the corresponding efficiencies decrease. This is apparently the reason for the non-Arrhenius behavior of τ_s [Fig. 5(a)], which corresponds to a pure elimination of NN antisite pairs by correlated pairs of Ni- and Al-atom ordering jumps.

After the saturation of the fast relaxation process, the relative increase of $P_{\text{Ni(Al)}:i\rightarrow j}$ with T_f appears stronger, while $E^{\text{ord}}_{\text{Ni(Al)}}$ decreases weaker, which disturbs the specific balance observed at the beginning of the relaxations. The main reason for the observed temperature dependence (Arrhenius behavior) of the rate of the slow process is, however, the fact that it involves Al-antisite migration, where the essential cases of the jumps coupling/uncoupling the NN antisite pairs cause nonzero energy changes ΔE. In addition, the normalized average minimum distance $\langle r^{(\text{eq})}_{\text{min}}\rangle_{\text{nor}}$ between single antisites (to be coupled and only then eliminated) decreases with temperature (see Fig. 8). As a result, the rate of the process shows certain temperature dependence yielding effectively positive activation energy.

2. Disordering

After an increase of temperature ($\Delta T>0$) the disordering jumps of Ni and Al-atoms simulated at the lowest value of $V^{(2)}_{\text{Al-Al}}$ (yielding the highest values of C) show almost similar initial frequencies and efficiencies [Figs. 9(d),9(e)]. This is a consequence of very close levels of the corresponding energy changes ΔE caused by Al- and Ni-atom jumps [Fig. 9(f)]. Such circumstances especially promote the fast increase of

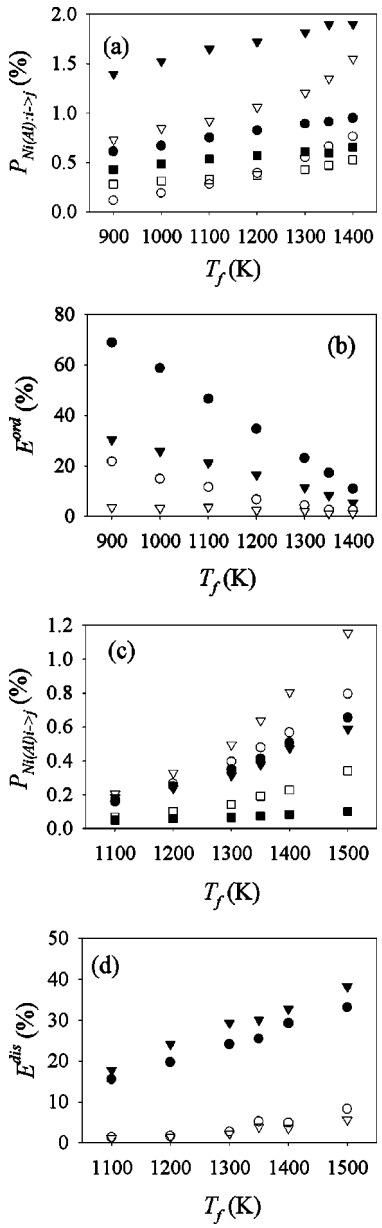

FIG. 15. Atomic-jump frequencies and efficiencies against the relaxation temperatures T_f at $V^{(1)}_{\text{Al-Al}}=-0.15$ eV and $V^{(2)}_{\text{Al-Al}}=-0.04$ eV. (a) Ordering: $P_{\text{Al:Ni}\to\text{Al}}$ (● and ○), $P_{\text{Ni:Al}\to\text{Ni}}$ (▼ and ▽), and $P_{\text{Al:Ni}\to\text{Ni}}$ (■ and □); (b) ordering: $E^{\text{ord}}_{\text{Al}}$ (● and ○) and $E^{\text{ord}}_{\text{Ni}}$ (▼ and ▽); (c) disordering: $P_{\text{Al:Al}\to\text{Ni}}$ (● and ○), $P_{\text{Ni:Ni}\to\text{Al}}$ (▼ and ▽) and $P_{\text{Al:Ni}\to\text{Ni}}$ (■ and □); (d) disordering: $E^{\text{dis}}_{\text{Al}}$ (● and ○) and $E^{\text{dis}}_{\text{Ni}}$ (▼ and ▽). (●, ■, ▼) denote the parameters averaged over initial 5000 MC steps/vacancy of relaxation, (○,□,▽) denote the same parameters averaged over 5000 MC steps/vacancy after the saturation of the fast component of relaxation.

APC, i.e., fast decrease of η proceeding according to Fig. 12. The process competes, however, with two effects.

Similar to the case of ordering, the existing NN antisite pairs are permanently uncoupled and recoupled due to the migration of the created Al antisites within the Ni sublattice. Each uncoupling of a NN antisite pair causes certain energy change ΔE which, as mentioned in the preceding paragraph, is positive and does not depend on $V^{(2)}_{\text{Al-Al}}$.

An increase of the number of Al antisites migrating over Ni sublattice [gradual increase of a profile of this process during the relaxation is visible in Fig. 11(a)] causes that they still more and more frequently approach the just created Al antisites and may jump with high probability to the just-created Al vacancies (instead of Ni atoms) stopping the creation of NN antisite pairs and also stopping the progress of fast disordering.

Further slow decrease of η (actually, active all through the relaxation) is accompanied by a *decrease* of APC [Fig. 7(c)] and, therefore, proceeds with a large contribution of Al-antisite migration in Ni sublattice (uncoupling of the NN antisite pairs). The uncoupling enables further disordering thanks to the formation of new NN antisite pairs [after the saturation of the fast $\eta(t)$ component], but also results in oscillations of the ''left-alone'' Ni antisites between the antisite and right positions, which is reflected by an increase of $P_{\text{Ni:Ni}\to\text{Al}}$ [Fig. 11(a)] and may lead to a definite elimination of a Ni antisite.

An increase of $V^{(2)}_{\text{Al-Al}}$ causes an increase of ΔE for Al-disordering jumps and a decrease of ΔE for the Ni disordering ones within the initial stage of relaxation [Fig. 9(f)]. For this reason, the disordering jumps of Al atoms become much rarer, but, being more often followed by Ni-atom jumps, are definitely more efficient [Fig. 9(e)]. Consequently, the effective rate of the production of NN antisite pairs $(1/\tau_s)$ remains constant [Fig. 6(d)].

A decrease of the weight factor C with increasing $V^{(2)}_{\text{Al-Al}}$ follows from the fact that on one hand the corresponding increase of ΔE for disordering jumps of Al atoms occurs without any substantial change of ΔE for Al antisite migration ones, including the cases of the uncoupling of NN antisite pairs, and on the other hand, the number of Al antisites continuously increases. Consequently, increased (and even inverted) is the difference between the frequencies $P_{\text{Al:Al}\to\text{Ni}}$ and $P_{\text{Al:Ni}\to\text{Ni}}$ and (i) more NN antisite pairs just created are very soon uncoupled and (ii) more Al vacancies just created by disordering Al-atom jumps are reached by previously created and migrating Al antisites. Both effects result in an earlier stop of the increase of APC.

Figure 15(c) shows that within the first 5000 MC steps/vacancy a decrease of the relaxation temperature T_f influences stronger the frequency of Al-disordering jumps than the frequency of Ni-disordering jumps. As a result, while at lower temperatures Ni atoms jump more frequently, Al-atom jumps dominate at higher T_f–the effect is analogous to the one at constant T_f and increasing $V^{(2)}_{\text{Al-Al}}$ [Fig. 9(d)]. At any T_f, however, Ni-atom jumps are more efficient [Fig. 15(d)]. The net effect is that the rate of the ''pure'' creation of NN antisite pairs $(1/\tau_s)$ does not change with T_f [Fig. 5(b)].

After the saturation of the fast relaxation process $P_{\text{Ni:Ni}\to\text{Al}}$ is always higher than $P_{\text{Al:Al}\to\text{Ni}}$ and increases with increasing T_f much stronger than does $P_{\text{Al:Al}\to\text{Ni}}$. However, at higher T_f the efficiency $E^{\text{dis}}_{\text{Al}}$ of Al-atom jumps becomes higher than $E^{\text{dis}}_{\text{Ni}}$. Therefore, the mechanism of ''compensation'' active within the first 5000 MC steps/vacancy of the relaxation does not work any more and the rate of the slow disordering $(1/\tau_l)$ shows temperature dependence.

Similarly as in the case of ordering, the main reason for a regular Arrhenius behavior of the longer relaxation time τ_l might be understood in terms of the positive ΔE for uncoupling of NN antisite pairs and of a decrease of the average minimum distance $\langle r_{\min}^{(eq)} \rangle$ between antisites with increasing temperature. After having been created as NN pairs, the antisites are now uncoupled (with positive ΔE) and moved in average by $\langle r_{\min}^{(eq)} \rangle$ before a new antisite pair is created. As a result, an increase of temperature is followed by a decrease of τ_l.

VI. CONCLUSIONS

(1) Monte Carlo computer simulations of order-order relaxations in the $L1_2$-long-range ordered intermetallic compound Ni_3Al based on the vacancy mechanism of atomic migration revealed a parallel operation of two coupled ''order-order'' relaxation modes observed in experiment: short-range ordering [time evolution of the antisite pair correlation (APC)] and long-range ordering (time evolution of the single-site correlation η).

(2) The predominating mechanism of any change of the degree of long-range order in the system, i.e., of the creation or elimination of antisite atoms observed, e.g., by means of resistometry,[1] is the creation (disordering) or elimination (ordering) of NN pairs of Ni and Al antisites by means of correlated jumps of Ni and Al atoms to NN vacancies (Fig. 12). This process is a mechanism for the simultaneous and correlated evolution of APC and η and shows up as the fast component of order-order relaxation in Ni_3Al.

(3) Although the concentration of the NN antisite-pairs (APC) is correlated with the concentration of antisites (η), at any temperature APC and η have independent equilibrium levels. The mechanism enabling the establishment of independent equilibria of APC and η is an easy migration of Al antisites within the Ni sublattice. Due to the Al-antisite migration the NN antisite pairs are permanently coupled (ordering) or uncoupled (disordering), which leads to and then maintains a dynamical equilibrium of APC and enables the possible further evolution of η towards its equilibrium level. The evolution of η enabled by the latter mechanism is observed as the slow component of order-order relaxation in Ni_3Al.

(4) It was shown that the contribution of the fast process to the order-order relaxation in a $L1_2$,-long-range-ordered A_3B system may be controlled by the values of input parameters used in the simulations—in particular, by the values of atomic pair-interaction energies. These parameters determine the balance between the frequencies of ordering/disordering ($P_{B:A\leftrightarrow B}$) and ''A-sublattice migration'' jumps ($P_{B:A\rightarrow A}$) of the minority B atoms within the initial stage of the process. The contribution of the fast process is reduced if $P_{B:A\rightarrow A}$ increases in relation to $P_{B:A\leftrightarrow B}$. Complete elimination of the fast process is, however, possible only in the case of disordering, where the NN antisite pairs are currently produced. If $P_{B:A\rightarrow A}$ is sufficiently high, this production may be at once compensated by the uncoupling mechanism. In the case of ordering, certain concentration APC of the NN antisite pairs to be quickly eliminated always exists in the system and, therefore, an increase of $P_{B:A\rightarrow A}$ causes only a limited reduction of the contribution of the fast process.

(5) The high correlation of the atomic jumps driving the fast relaxation of η is the reason for the irregular behavior of its *simulated* relaxation time (no definite temperature dependence). However, the effect is supposed to result from the specific algorithm and model applied in the performed computer simulations.

The study is currently continued by means of Monte Carlo and Molecular Dynamics simulations with ''embedded-atom'' (EAM) potentials for particular intermetallic compounds. It aims at the estimation of average saddle-point energies for atomic jumps, which are then used as input parameters in MC simulations run with various algorithms. Preliminary simulations of order-order relaxations in Ni_3Al run using Glauber [Eq. (1.1)] and ''residence-time''[39] algorithms with EAM potentials yielded qualitatively similar results as those reported in the present paper (coexistence of two LRO relaxation processes correlated with the specific APC kinetics).[40]

ACKNOWLEDGMENTS

The simulations were partially performed on two super computers: a convex Exemplar SPP 1600/XA (Grant No. KBN/SPP/UJ/036/1995) and HP Exemplar S2000 (Grant No. KBN/S2000/UJ/047/1998) both localized at the CYFRONET (Cracow, Poland). The work was partially supported by State Committee for Scientific Research (Grant No. 2P03B 088 19) and the governments of France (Grant No. 76411) and Austria (Grant No. 96022).

[1] R. Kozubski, Prog. Mater. Sci. **41**, 1 (1997).

[2] R. Kozubski and M.C. Cadeville, J. Phys. F: Met. Phys. **18**, 2569 (1988).

[3] C. Dimitrov, X. Zhang, and O. Dimitrov, Acta Mater. **44**, 1691 (1996).

[4] G. Sattonay and O. Dimitrov, Acta Mater. **47**, 2077 (1999).

[5] K. Rohrhofer, H. Lang, P. Rosenkranz, R. Kozubski, W. Pueschl, and W. Pfeiler, in *High-Temperature Ordered Intermetallic Alloys VIII*, edited by E. P. George *et al.*, MRS Symposia Proceedings No. 552 (Materials Research Society, Pittsburgh, 1999).

[6] R.W. Cahn, P.A. Siemers, J.E. Geiger, and P. Bardhan, Acta Metall. Mater. **35**, 2737 (1987).

[7] W. Pfeiler, H. Lang, W. Pueschl, and R. Kozubski, in *Solid-Solid Phase Transformations*, edited by M. Koiwa, K. Otsuka, and T. Miyazaki, Proceedings Vol. 12 (JIMIC'3) (The Japan Institute of Metals, Tokyo, 1999), p. 457.

[8] F. Willaime and C. Massobrio, in *Defects in Materials*, edited by P.D. Bristome *et al.*, MRS Symposia Proceedings No. 209 (Materials Research Society, Pittsburgh, 1991), p. 293.

[9] *Monte Carlo Methods in Statistical Physics* edited by K. Binder,

(Springer, Berlin, 1979).
[10] N. Metropolis, A.W. Rosenbluth, M.N. Rosenbluth, A.H. Teller, and E. Teller, J. Chem. Phys. **21**, 1087 (1953).
[11] R.J. Glauber, J. Math. Phys. **4**, 294 (1963).
[12] A. Flinn and P.G.M. McManus, Phys. Rev. **124**, 54 (1961).
[13] J.R. Beeler, Phys. Rev. **138**, A1259 (1965).
[14] K. Yaldram, V. Pierron-Bohnes, M.C. Cadeville, and M.A. Khan, J. Mater. Res. **10**, 1 (1995).
[15] E. Kentzinger, M. Zemirli, V. Pierron-Bohnes, M.C. Cadeville, H. Bouzar, M. Benakki, and M.A. Khan, Mater. Sci. Eng., A **239**, 784 (1997).
[16] V.I. Gorentsveig, P. Fratzl, and J.L. Lebovitz, Phys. Rev. B **55**, 2912 (1997).
[17] C. Frontera, E. Vives, and A. Planes, Z. Phys. B: Condens. Matter **96**, 79 (1994).
[18] J.Ph. Jay, M. Wojcik, and P. Panissod, Z. Phys. B: Condens. Matter **101**, 471 (1996).
[19] A.G. Khachaturyan, Sov. Phys. Solid State **9**, 2040 (1968).
[20] L.-Q. Chen and A.G. Khachaturyan, Acta Metall. Mater. **39**, 2533 (1991).
[21] A.M. Mebed, T. Koyama, and T. Miyazaki, J. Mater. Sci. **32**, 5797 (1997).
[22] R. Poduri and L.-Q. Chen, Acta Mater. **46**, 1719 (1998).
[23] G. Yu, and K. Luecke, Acta Metall. Mater. **40**, 2523 (1992).
[24] A.M. Gusak, and A.O. Kovalchuk, Phys. Rev. B **58**, 2551 (1998).
[25] C. Pareige, F. Soisson, G. Martin, and D. Blavette, Acta Mater. **47**, 1889 (1999).
[26] Y. Limoge and J.L. Bocquet, Acta Metall. **36**, 1717 (1988).
[27] K. Badura-Gergen and H.-E. Schaefer, Phys. Rev. B **56**, 3032 (1997).
[28] P. Oramus, R. Kozubski, M.C. Cadeville, V. Pierron-Bohnes, and W. Pfeiler, in *Diffusion Mechanisms in Crystalline Materials*, edited by Y. Mishin *et al.*, MRS Symposia Proceedings No. 527 (Materials Research Society, Pittsburgh, 1998), p. 185.
[29] P. Oramus, R. Kozubski, M.C. Cadeville, V. Pierron-Bohnes, and W. Pfeiler, Acta Phys. Pol. A **96**, 153 (1999).
[30] S.B. Debiaggi, P.M. Decorte, and A.M. Monti, Phys. Status Solidi B **195**, 37 (1996).
[31] H. Numakura, N. Kurita, and M. Koiwa, in *Solid-Solid Phase Transformations* (Ref. 7), p. 465.
[32] G. Neumann, Phys. Status Solidi B **144**, 329 (1987).
[33] S.M. Kim, J. Mater. Res. **6**, 1455 (1991).
[34] P. Cenedese, A. Marty, and Y. Calvayrac, J. Phys. (France) **50**, 2193 (1989).
[35] B. Fultz, J. Mater. Res. **5**, 1419 (1990).
[36] L.-Q. Chen, Phys. Rev. B **58**, 5266 (1998).
[37] K. Gschwend, H. Sato, and R. Kikuchi, J. Chem. Phys. **69**, 5006 (1978).
[38] K.F. Ludwig, G.B. Stephenson, J.L. Jordan-Sweet, J. Mainville, Y.S. Yang, and M. Sutton, Phys. Rev. Lett. **61**, 1859 (1988).
[39] F. Haider, in *Ordering and Disordering in Alloys*, edited by A.R. Yavari (Elsevier, Barking, 1992), p. 215.
[40] P. Oramus, R. Kozubski, V. Pierron-Bohnes, M.C. Cadeville, C. Massobrio, and W. Pfeiler, Mater. Sci. Eng. A (to be published).